



On the absorption rate of membrane-based adiabatic sorber beds: An analytical approach

Mahyar Ashouri, Majid Bahrami*

Laboratory for Alternative Energy Conversion (LAEC), School of Mechatronic Systems Engineering, Simon Fraser University, Surrey, Canada, and Pacific Institute for Climate Solutions (PICS)



ARTICLE INFO

Article history:

Received 14 July 2022

Revised 15 February 2023

Accepted 15 March 2023

Available online 21 March 2023

Keywords:

Absorber and desorber

Analytical solution

Heat and mass transfer

Hollow fiber membrane

Membrane

ABSTRACT

Membrane-based sorber beds play a key role in numerous engineering applications. As an emerging design, adiabatic membrane-based sorber beds can provide compact heat and mass exchangers. For the first time, this study presents two analytical solutions for coupled heat and mass transfer in the flat and hollow fiber membrane-based adiabatic sorber beds used in absorption heat pump/chiller applications. The similarity solution and Laplace transform method are used to develop the analytical models. The proposed models are validated with experimental data and numerical results available in the literature. In addition, a parametric study is performed to analyze the impact of operating conditions and the physical properties of membrane on the absorption rate. Based on the parametric study, the solution inlet concentration is the most effective parameter for increasing the absorption rate. Also, porosity is the key membrane property for enhancing absorption rate. It is shown that the absorption rate of a flat membrane-based sorber bed is higher than that of a hollow fiber membrane-based sorber bed under the same conditions.

© 2023 Elsevier Ltd. All rights reserved.

1. Introduction

Climate change is one of the most significant concerns of the world in recent decades. Cooling and heating systems account for about 50% of the energy demand of commercial and residential buildings [1]. Consumed as the primary energy source in industrial processes and residential buildings, fossil fuels are one of the major sources of greenhouse gas emissions [2,3]. Also, recognized as an ozone-depleting potential, fluorocarbon-type refrigerants, which are implemented in vapor compression refrigeration systems, aggravate the climate change crisis [4,5].

Heat-driven absorption chillers/heat pumps are considered as an alternative to address the mentioned issues. Using environmentally friendly working fluids, absorption chillers/heat pumps can operate with low-grade heat – which is about 52% of the global primary energy [6]. However, because they have a low Coefficient of Performance (COP) and high cost, available absorption chillers/heat pumps are not able to compete with vapor compression refrigeration systems [7]. Sorber beds, or absorbers/desorbers, significantly affect the COP, size, and cost of

absorption chillers/heat pumps, since absorption and desorption rates are the most performance-limiting factors [8].

To increase the absorption rate, several sorber bed configurations have been proposed so far: i) bubbly flows; ii) the use of spray nozzles; and iii) falling films [9]. These configurations have failed to significantly improve the performance and led to heavy, oversized, and inefficient heat and mass exchangers. Large film thickness, flow separation, and low surface wetting ratio are the main issues plaguing the performance of conventional sorber beds. Recently, membrane-based sorber beds have received immense attention for improving the COP and lowering the cost and size of absorption chillers/heat pumps [10]. Typically, microporous/nanofiber membranes are used to separate the liquid and gaseous phases. The liquid phase cannot penetrate the hydrophobic membrane, yet the gaseous phase can, resulting in water vapor absorption or desorption.

Membrane-based sorber beds can be categorized into two types: i) the isothermal membrane-based sorber beds in which the solution film is continuously cooled or heated via a heat transfer fluid; and ii) the adiabatic membrane-based sorber beds in which the solution film is not cooled or heated via a heat transfer fluid during absorption process. Isothermal membrane-based sorber beds have been investigated numerically, theoretically, and experimentally [11,12,21–26,13–20]. Isothermal membrane-based sorber beds have shown promising performance; however, adiabatic

* Corresponding author.

E-mail address: mbahrami@sfu.ca (M. Bahrami).

Nomenclature

Abbreviations

COP	Coefficient of performance
HFMA	Hollow Fiber Membrane-based Absorber
HFMD	Hollow Fiber Membrane-based Desorber
HFM	Hollow Fiber Membrane
FMAA	Flat Membrane-based Adiabatic Absorber
FMAD	Flat Membrane-based Adiabatic Desorber
A_c	Channel cross-section area, m^2
c	Concentration of absorbate, $kg \cdot kg^{-1}$
c	Isobaric specific heat, $J \cdot kg^{-1} K^{-1}$
D	Mass diffusivity, $m^2 \cdot s^{-1}$
D_m	Membrane mean pore diameter, μm
g	Gravity, $m \cdot s^{-2}$
h_{abs}	Absorption heat
J	Mass flux, $kg \cdot m^{-2} \cdot s^{-1}$
k_m	Membrane mass transfer coefficient, $kg \cdot m^{-2} \cdot s^{-1} \cdot Pa^{-1}$
p	Pressure, Pa
Le	Lewis number, $[Le = \alpha \cdot D^{-1}]$
L_m	Membrane length, m
M	Molecular mass, $g \cdot mol^{-1}$
\dot{m}	Mass flux, $kg \cdot m^{-2} \cdot s^{-1}$
\dot{q}	Heat flux, $W \cdot m^{-2}$
R	Universal gas constant, $J \cdot mol^{-1} K^{-1}$
T	Temperature, K
\bar{u}	Average velocity, $m \cdot s^{-1}$
x, y	Local tangential and normal position, m

Greek symbols

α	Thermal diffusivity, $m^2 \cdot s^{-1}$
φ	Membrane porosity
γ	Dimensionless mass fraction
Y	Dimensionless mass fraction in the Laplace space
η	Dimensionless normal position
Λ	Normalized heat of absorption
τ	Membrane tortuosity
θ	Dimensionless temperature
Θ	Dimensionless temperature in the Laplace space
δ	Film thickness, μm
δ_m	Membrane thickness, μm
ρ	Density, $kg \cdot m^{-3}$

Subscripts

eq	Equilibrium
m	Membrane
inf	Interface
o	Inlet
s	Solution
v	Vapor
w	Wall

membrane-based sorber beds have exhibited comparable performance while being more compact and less costly. Consequently, adiabatic membrane-based sorber beds can also be considered as a promising option for applications, such as automotive industry. Adiabatic membrane-based sorber beds include two types: i) flat membrane-based adiabatic sorber beds; and ii) hollow fiber membrane-based adiabatic sorber beds.

Venegas et al. [27] performed a 1-D numerical simulation to analyze the performance of a flat membrane-based adiabatic absorber. They compared the flat membrane-based adiabatic performance to an isothermal membrane-based absorber. The absorption rate of their flat membrane-based adiabatic absorber

($0.0023 \text{ kg/m}^2 \cdot s$) was almost 70% of their isothermal membrane-based absorber ($0.0033 \text{ kg/m}^2 \cdot s$) under the same operating conditions and geometrical parameters. García-Hernando et al. [28] analyzed the effect of membrane physical properties on the performance of a flat membrane-based adiabatic absorber. Three different nanofibrous membranes, including FALP29325, PTU0453001, and PTFE0453005 were tested. An LiBr-water solution was used as the working fluid. A maximum absorption rate of $0.0026 \text{ kg/m}^2 \cdot s$ was obtained in this study. It was reported that decreasing the mean pore diameter and increasing the membrane thickness resulted in lower absorption rates. In another study, García-Hernando et al. [29] experimentally investigated the effect of operating conditions on the flat membrane-based adiabatic absorber's performance. The LiBr-water was used as the solution. The flat membrane-based adiabatic absorber was fabricated with 50 rectangular microchannels that were 0.15 mm in height, 3 mm in width, and 58 mm in length. A microporous polytetrafluoroethylene (PTFE) membrane was used with a thickness of $100 \mu m$, a mean pore diameter of $0.45 \mu m$, and a porosity of 0.9 . The maximum absorption rate of $0.0038 \text{ kg/m}^2 \cdot s$ was obtained in this study. Additionally, increasing the solution mass flow rate and vapor pressure led to higher absorption rates.

Hollow fiber membrane reactors have been further studied for CO_2 capture [30]. Recently, this technology has also been studied as a promising alternative for sorber beds in absorption chillers/heat pumps [31,32]. Hong et al. [33] proposed a novel absorption refrigeration system for automobile applications, where a hollow fiber membrane was used to design the desorber. They numerically modeled the system and showed that a cooling capacity and a COP of approximately 2.88 kW and 0.63 , respectively, can be achieved. In another study, Hong et al. [34] experimentally studied the impact of operating conditions on the performance of a hollow fiber membrane-based adiabatic desorber. Microporous hollow fiber membranes with an inner diameter of $390 \mu m$, a mean pore diameter of $0.16 \mu m$, and a porosity of 0.5 were used. A maximum desorption rate of about $0.0014 \text{ kg/m}^2 \cdot s$ was obtained. Also, increasing the solution mass flow rate and solution inlet temperature enhanced the desorption rate. On the other hand, decreasing the vapor pressure and the solution inlet concentration led to higher desorption rates. Wang et al. [35] experimentally analyzed a hollow fiber membrane-based adiabatic desorber made of polyvinylidene fluoride which was used in an absorption chiller. They stated that using hollow fiber membranes could result in the fabrication of a compact, inexpensive, and efficient desorber.

Computational fluid dynamics and numerical methods can be utilized to model the present system. However, they require a high computational cost, and the restriction of their results to specific selected operating conditions and geometrical parameters reduces their usability when the source code is not accessible. On the other hand, precise analytical solutions [36] can be a key for optimization, real-time control, and parametric study in a time-efficient fashion. Furthermore, the physics of the phenomenon can be comprehensively captured via analytical solutions.

To the best of the authors' knowledge, there is no analytical study for coupled heat and mass transfer in flat membrane-based adiabatic sorber beds. Regarding hollow fiber membrane-based adiabatic sorber beds, although, there are some analytical solutions for hollow fiber membrane contactors for liquid desiccant air dehumidification [37] and CO_2 capture [38], they cannot be used for absorption chiller/heat pump applications. The previous studies assume that the gaseous phase (i.e. air to be dehumidified or biogas to be upgraded) has a velocity parallel to the solution flow direction, coming from the inlet and going out from the outlet [37]. Thus, using one-dimensional modeling and integrating control volumes from the inlet to the outlet, the absorption

rate can be found [37]. However, in this application, there is either inlet (for absorber) or outlet (for desorber) [34]. The water vapor surrounding the hollow fiber membrane has a very low radial velocity (normal to the solution direction). Accordingly, the previous models cannot be applied to this application and using those analytical models results in a zero absorption rate for this application.

For the first time, the present study proposes two analytical solutions for heat and mass transfer in flat and hollow fiber membrane-based adiabatic sorber beds used in absorption chillers and heat pumps. The similarity solution approach and the Laplace transform method are used to find closed-form solutions for the heat and mass transfer in flat and hollow fiber membrane-based sorber beds, respectively. The models are validated with the numerical studies and experimental data available in the literature. The impact of the operating conditions, i.e., vapor pressure, film thickness, channel length, solution mass flow rate, inlet concentration and temperature along with the physical properties of membrane (porosity, mean pore diameter, and thickness) are studied using the developed models. Also, the absorption rate of flat and hollow fiber membrane-based adiabatic sorber beds are compared under similar conditions.

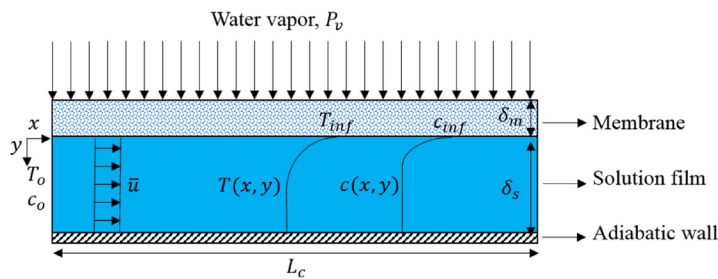
2. Problem description and assumptions

Coupled heat and mass transfer in flat and hollow fiber membrane-based adiabatic sorber beds are investigated, as schematically indicated in Fig. 1. The most common solution in absorption chillers/heat pumps, LiBr-water, is selected as the working fluid. In a flat membrane-based adiabatic sorber bed, the LiBr-water solution film is confined by a plate and a microporous/nanofiber membrane. In a hollow fiber membrane-based adiabatic sorber bed, the LiBr-water solution flows in hollow fiber membranes. The membrane is impermeable to the LiBr-water so-

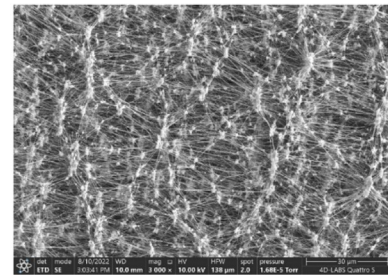
lution but not to vapor, resulting in vapor absorption or desorption at the membrane-solution interface.

To develop the analytical models, the following assumptions are made [40]:

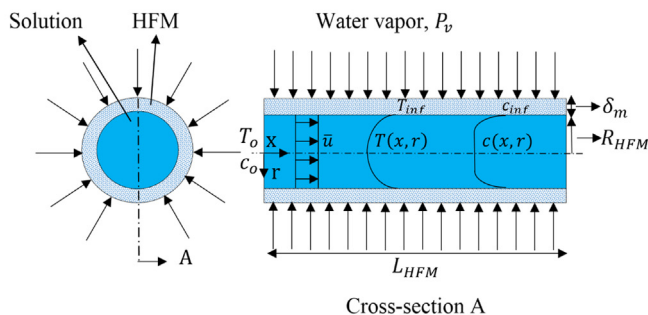
- The solution film is laminar ($Re \sim 1 \ll 2300$);
- The flow is hydrodynamically fully-developed since the developing length ($L_{developing} = 0.57 * D * Re$ [41]) does not exceed 1 mm; a developing length of less than 5% of the entire length is preferable;
- A linear estimation is used to find the pressure as a function of the solution temperature and concentration at the solution-membrane interface; a relative difference of less than 10% for the fitted plane is preferable for the desired absorbent to estimate the pressure;
- The mean velocity is used rather than a parabolic velocity profile;
- The thermo-physical properties of the solution are assumed to be constant, i.e., an averaged value for each property may be used over the corresponding temperature and concentration range.
- The heat transfer from the film to the gaseous phase and membrane is negligible due to the vacuum condition and very low water vapor velocity;
- The inlet concentration and temperature distributions are uniform and constant;
- The absorbent is non-volatile;
- The absorption process is physical meaning that it occurs because of the pressure difference between the vapor phase and vapor partial pressure at the interface.
- The membrane temperature is constant; and
- The desorption temperature should be less than the boiling point of the solution (i.e. nearly 95°C for aqueous LiBr [15]).



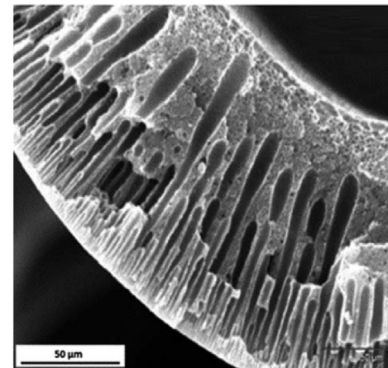
(a)



(b)



(c)



(d)

Fig. 1. Schematic diagram of: (a) a flat membrane-based adiabatic sorber bed; (b) an SEM image of a PTFE membrane; (c) a hollow fiber membrane-based (HFM) adiabatic sorber bed; and (d) an SEM image of a hollow fiber membrane [39].

3. Model development

3.1. Mass transfer through a membrane

Molar diffusion and viscous fluxes account for the mass transfer through a membrane. Accordingly, the Dusty-Gas model [17,42] is used to calculate the mass transfer rate, J , through the membrane:

$$J = k_m(p_v - p_{inf}) \left[\frac{\text{kg}}{\text{m}^2 \cdot \text{s}} \right] \quad (1)$$

where, p_v , p_{inf} , and k_m denote vapor pressure, vapor partial pressure at the interface, membrane mass transfer coefficient, and membrane mass transfer coefficient, respectively, which is obtained as follows:

$$k_m = -\frac{\varphi D_m}{\delta_m \tau} \left(\sqrt{\frac{8M}{9\pi R T_m}} + \frac{p_v D_m}{32 \mu_g R T_m} \right) \left[\frac{\text{kg}}{\text{Pa} \cdot \text{m}^2 \cdot \text{s}} \right] \quad (2a)$$

$$T_m = \frac{T_o + T_v}{2} [K] \quad (2b)$$

$$\tau = \frac{(2 - \varphi)^2}{\varphi} \quad (2c)$$

where, φ , D_m , τ , and δ_m are the membrane porosity, pore mean diameter, tortuosity, and thickness, respectively. In addition, M , R , T_m , and μ_g are the vapor molar weight, universal gas constant, membrane average temperature, and vapor dynamic viscosity, respectively.

3.2. Governing equations

Due to assuming a hydrodynamically fully-developed flow and mean velocity, it is not required to solve the continuity and Navier-Stocks equations for the solution, and the mean velocity is calculated as follows:

$$\bar{u} = \frac{\dot{m}_s}{\rho_s A_c} \left[\frac{m}{s} \right] \quad (3)$$

where, \dot{m}_s , A_c , and ρ_s are the mass flow rate of the solution, the solution channel or hollow fiber membrane cross sectional area, and the solution density, respectively. Considering the convective and advective transports parallel to the flow direction and diffusivity transport perpendicular to the "y" direction, the governing equations and boundary conditions for the conservation of energy and species are shown in Table 1.

The vapor partial pressure at the membrane-solution interface " p_{inf} " for the LiBr-water solution is obtained using an experimental correlation proposed by Matsuda et al. [44]:

$$p_{inf}(T_{inf}, c_{inf}) = \exp \left(A(c_{inf}) + \frac{B(c_{inf})}{T_{inf}} + \frac{C(c_{inf})}{T_{inf}^2} \right) \quad (17)$$

See Appendix A for the corresponding constants in Eq. (17). Temperature and concentration ranges are limited in real applications. As it has been explained in our previous study, see Ref. [40], the membrane-solution interface pressure can be estimated as a linear function of the solution concentration and temperature. For instance, to validate the present study with Ref. [27], the interface pressure can be calculated as $p_{inf} = -1.643 \times 10^4 + 42.65 T + 9320 c$, within $0.4 < c < 0.45$ and $305 K < T < 314 K$, with a relative difference of 5.3%. Accordingly, a general estimation for the membrane-solution interface pressure " p_{inf} " can be expressed as follows [40]:

$$p_{inf} = b_0 + b_1 T_{inf} + b_2 c_{inf} \quad (18)$$

The corresponding constants for a specific range of concentration and temperature can be calculated using a curve fitting process. By substituting Eq. (18) in Eq. (14), Eq. (14) is converted to:

$$b_3 \frac{\partial \gamma}{\partial \eta} |_{inf} = k_m(p_v - b_4 \theta_{inf} - b_5 \gamma_{inf} - p_o) \quad (19a)$$

$$b_3 = \frac{\rho_s D_s c_o}{\delta} \quad (19b)$$

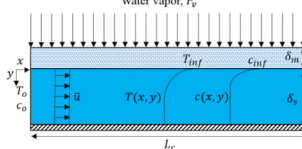
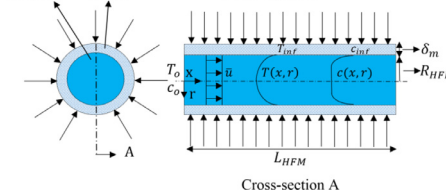
$$b_4 = b_1 T_o \quad (19c)$$

Table 1
Governing equations and boundary conditions for energy and species conservations [40,43].

Geometry	Flat membrane-based adiabatic sorber bed	Hollow fiber membrane-based (HFM) adiabatic sorber bed
	<p>Cartesian coordinate</p> $\bar{u} \frac{\partial T}{\partial x} = \alpha_s \frac{\partial^2 T}{\partial y^2}$ $\bar{u} \frac{\partial c}{\partial x} = D_s \frac{\partial^2 c}{\partial y^2}$ $\frac{\partial \theta}{\partial \xi} = \frac{\partial^2 \gamma}{\partial \eta^2}$ $Le \frac{\partial \gamma}{\partial \xi} = \frac{\partial^2 \gamma}{\partial \eta^2}$ $\theta(\xi, \eta) = \frac{T(\xi, \eta) - T_o}{T_o - T_o}$ $\gamma(\xi, \eta) = \frac{c(\xi, \eta) - c_o}{c_o - c_o}$ $\xi = \frac{x}{\delta_s^2} \bar{u} \quad \& \quad \eta = \frac{y}{\delta_s}$ $\theta(0, \eta) = \frac{T_o - T_o}{T_o - T_o} = 0$ $\gamma(0, \eta) = \frac{c_o - c_o}{c_o - c_o} = 0$ $\frac{\partial \theta}{\partial \eta} _{\eta=1} = 0$ $\frac{\partial \gamma}{\partial \eta} _{\eta=1} = 0$ $\frac{\rho_s D_s c_o}{\delta} \frac{\partial \gamma}{\partial \eta} _{inf} = k_m(p_v - p_{inf})$ $\frac{\partial \theta}{\partial \eta} _{inf} = \frac{\Delta}{Le} \frac{\partial \gamma}{\partial \eta} _{inf}$ <p>Non-dimensional numbers</p> $\Lambda = \frac{h_{m,s} c_o}{c_o T_o}$	<p>Cylindrical coordinate</p> $\bar{u} \frac{\partial T}{\partial x} = \alpha_s \left(\frac{\partial^2 T}{\partial r^2} + \frac{1}{r} \frac{\partial T}{\partial r} \right)$ $\bar{u} \frac{\partial c}{\partial x} = D_s \left(\frac{\partial^2 c}{\partial r^2} + \frac{1}{r} \frac{\partial c}{\partial r} \right)$ $\frac{\partial \theta}{\partial \xi} = \frac{\partial^2 \gamma}{\partial \eta^2} + \frac{1}{\eta} \frac{\partial \theta}{\partial \eta}$ $Le \frac{\partial \gamma}{\partial \xi} = \frac{\partial^2 \gamma}{\partial \eta^2} + \frac{1}{\eta} \frac{\partial \gamma}{\partial \eta}$ $\theta(\xi, \eta) = \frac{T(\xi, \eta) - T_o}{T_o - T_o}$ $\gamma(\xi, \eta) = \frac{c(\xi, \eta) - c_o}{c_o - c_o}$ $\xi = \frac{x}{R_{HFM}^2} \bar{u} \quad \& \quad \eta = \frac{r}{R_{HFM}}$ $\theta(0, \eta) = \frac{T_o - T_o}{T_o - T_o} = 0$ $\gamma(0, \eta) = \frac{c_o - c_o}{c_o - c_o} = 0$ $\frac{\partial \theta}{\partial \eta} _{\eta=0} = 0$ $\frac{\partial \gamma}{\partial \eta} _{\eta=0} = 0$ $\frac{\rho_s D_s c_o}{R_{HFM} \delta} \frac{\partial \gamma}{\partial \eta} _{inf} = k_m(p_v - p_{inf})$ $\frac{\partial \theta}{\partial \eta} _{inf} = \frac{\Delta}{Le} \frac{\partial \gamma}{\partial \eta} _{inf}$ $Le = \frac{\alpha_s}{D_s}$

Table 2

The proposed equations for the heat and mass transfer in flat and hollow fiber membrane-based (HFM) adiabatic sorber bed.

Geometry	Parameter
<p>Flat membrane-based adiabatic sorber bed</p> 	$\dot{q}(\xi) = \frac{k_s T_o}{\delta_s \sqrt{\pi \xi}} \tilde{\theta}_{inf} \left[\frac{W}{m^2} \right] \quad (22)$ $\dot{m}(\xi) = \frac{\rho_s D_s c_o}{\delta_s} \sqrt{\frac{Le}{\pi \xi}} \tilde{\gamma}_{inf} \left[\frac{kg}{m^2 \cdot s} \right] \quad (23)$
<p>Hollow fiber membrane-based adiabatic sorber bed</p> 	$\dot{q}(\xi) = \frac{k_s T_o}{R_{HFM}} \frac{\partial (ILT(\Theta(s, \eta=1)))}{\partial \eta} \Big _{inf} \left[\frac{W}{m^2} \right] \quad (24)$ $\dot{m}(\xi) = \frac{\rho_s D_s c_o}{R_{HFM}} \frac{\partial (ILT(\Upsilon(s, \eta=1)))}{\partial \eta} \Big _{inf} \left[\frac{kg}{m^2 \cdot s} \right] \quad (25)$
$\tilde{\gamma}_{inf} = \left[\frac{k_m (p_o - p_o)}{k_m b_5 + 2 \frac{b_3 \sqrt{Le}}{\sqrt{\pi \xi}} + \frac{k_m b_4 \Lambda}{\sqrt{Le}}} \right] \tilde{\theta}_{inf} = \frac{\Lambda}{\sqrt{Le}} \left[\frac{k_m (p_o - p_o)}{k_m b_5 + 2 \frac{b_3 \sqrt{Le}}{\sqrt{\pi \xi}} + \frac{k_m b_4 \Lambda}{\sqrt{Le}}} \right] \quad (26)$	
$\Theta(s, \eta) = \left[\frac{\Lambda}{\sqrt{Le}} \frac{I_1(\sqrt{Le} \cdot s)}{I_1(\sqrt{s})} \right] \left[\frac{k_m (p_o - p_o)}{b_3 \sqrt{Le} \cdot s I_1(\sqrt{Le} \cdot s) + k_m b_4 \frac{\Lambda}{\sqrt{Le}} \frac{I_1(\sqrt{Le} \cdot s)}{I_1(\sqrt{s})} I_0(\sqrt{s}) + k_m b_5 I_0(\sqrt{Le} \cdot s)} \right] I_0(\sqrt{s} \eta) \quad (27)$	
$\Upsilon(s, \eta) = \left[\frac{k_m (p_o - p_o)}{b_3 \sqrt{Le} \cdot s I_1(\sqrt{Le} \cdot s) + k_m b_4 \frac{\Lambda}{\sqrt{Le}} \frac{I_1(\sqrt{Le} \cdot s)}{I_1(\sqrt{s})} I_0(\sqrt{s}) + k_m b_5 I_0(\sqrt{Le} \cdot s)} \right] I_0(\sqrt{Le} \cdot s \eta) \quad (28)$	
$\Lambda = \frac{h_{ab} c_o}{c_s l_o} \quad Le = \frac{\alpha_s}{D_s} \quad \text{ILT: Inverse Laplace Transform (see Appendix C.)}$	

$$b_5 = b_2 c_o \quad (19d)$$

$$p_o = b_0 + b_1 T_o + b_2 c_o \quad (19e)$$

It should be mentioned that "p_o" is the solution vapor pressure at the solution initial temperature and concentration ("T_o" and "c_o"). To obtain more accurate results, it is recommended that "p_o" be directly calculated from the correlation in Eq. (17). See Appendices B and C for more details.

Heat and mass transfer rates are calculated using the temperature and concentration profiles:

$$\dot{q}(\xi) = \frac{k_s T_o}{\delta_s} \left(\text{or } R_{HFM} \right) \frac{\partial \theta}{\partial \eta} \Big|_{inf} \left[\frac{W}{m^2} \right] \quad (20)$$

$$\dot{m}(\xi) = \frac{\rho_s D_s c_o}{\delta_s} \left(\text{or } R_{HFM} \right) \frac{\partial \gamma}{\partial \eta} \Big|_{inf} \left[\frac{kg}{m^2 \cdot s} \right] \quad (21)$$

The developed closed-form solutions for the heat and mass transfer in flat and hollow fiber membrane-based adiabatic sorber beds are shown in Table 2.

4. Results and discussion

4.2. Comparison with experimental data

The developed models for the heat and mass transfer in flat and hollow fiber membrane-based adiabatic sorber beds are validated with the experimental data of García-Hernando et al. [28] and Hong et al. [34], and the numerical results of Venegas et al. [27]. Table 3 represents the operating conditions and geometrical parameters of Ref. [27,28,34] used for validating the current models. Also, Table 4 lists the thermophysical properties of the aqueous LiBr.

Fig. 2 shows a comparison between the present models for the heat and mass transfer in flat and hollow fiber membrane-based adiabatic sorber beds against the numerical results of Venegas et al. [27] and the experimental data of García-Hernando et al.

Table 3

Operating conditions for the experimental and numerical data used for the validation [27,28,34].

Reference	Venegas et al. [27]	García-Hernando et al. [28]	Hong et al. [34]
Inlet temperature (°C)	32	27	65–83
Solution inlet concentration (kg/kg)	0.6	0.6	0.51–0.53
Mass flow rate (kg/h)	1.8	0.7–1	25
Number of channels or hollow fiber membranes	16	50	380
Absorber chamber pressure (kPa)	1	1.8–2.3	4.7
Solution channel length (mm)	30	58	250
Film thickness (μm)	150	150	195
Membrane thickness or hollow fiber membrane radius (μm)	60	38	75
Membrane porosity	0.8	0.9	0.5
Membrane mean pore diameter (μm)	1	0.45	0.16

Table 4

Thermal properties of aqueous LiBr [45,46].

Parameter	Value
Heat of absorption (kJ/kg)	2500
Lewis number	45–100
Solution thermal conductivity (W/m.K)	0.42–0.48
Solution specific heat (J/kg.K)	2000
Solution density (kg/m ³)	1500–1750

[28] and Hong et al. [34]. The minimum, average, and maximum relative differences of the proposed model compared to Refs. [27,28,34] are presented in Table 5. As can be seen, the proposed models follow the trend in data and show good agreement.

4.3. Parametric study

In this section, the impact of the operating conditions and the physical properties of membrane on the absorption and desorption

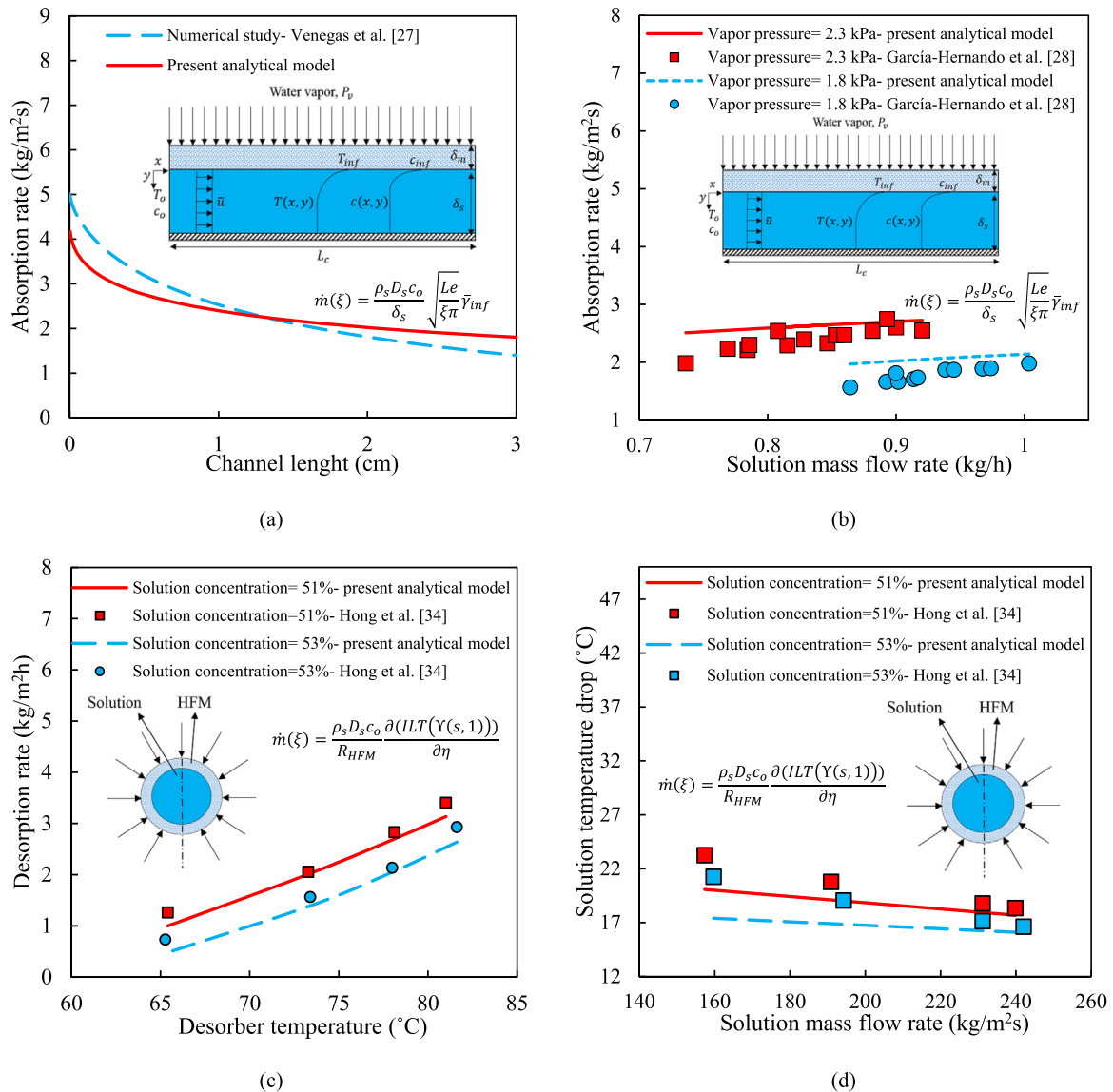


Fig. 2. The comparison between the results from the similarity solution method used for the flat membrane-based adiabatic absorber against: (a) the numerical result of Venegas et al. [27]; and (b) the experimental data of García-Hernando et al. [28]. Also, the comparison between the present Laplace transform model for the hollow fiber membrane-based (HFM) adiabatic desorber against: (c); and (d) the experimental data of Hong et al. [34].

Table 5

Minimum, average, and maximum relative difference between the present models compared to Refs. [27,28,34].

Study		Min. relative difference (%)	Averaged relative difference (%)	Max. relative difference (%)
Venegas et al. [27]	Fig. 3(a)	0	12.7	28.7
García-Hernando et al. [28]	Fig. 3 (b)	1.7	15.3	26.5
Hong et al. [34]	Fig. 3 (c)	2.2	12	29.1
	Fig. 3 (d)	5.3	7.9	12.4

Table 6

Baseline operating conditions and the physical properties of membrane used for the parametric study.

Parameter	Absorber		Desorber	
	Value	Range	Value	Range
Inlet temperature (°C)	27.5	24.75–30.25 (±10%)	80	72–88 (±10%)
Inlet concentration (kg water/kg solution)	0.4	0.4–0.44 (+10%)	0.5	0.46–0.5 (–10%)
Average velocity (m/s)	0.02	0.016–0.024 (±20%)	0.02	0.016–0.024 (±20%)
Vapor pressure (Pa)	1000	800–1200 (±20%)	5000	4000–6000 (±20%)
Film thickness in channel or hollow fiber membrane radius (μm)	150	120–180 (±20%)	150	120–180 (±20%)
Membrane thickness (μm)	60	48–72 (±20%)	60	48–72 (±20%)
Membrane porosity	0.8	0.48–0.96 (–40%/+20%)	0.8	0.48–0.96 (40%/+20%)
Membrane mean pore diameter (μm)	1	0.5–1.5 (±50%)	1	0.5–1.5 (±50%)
Solution channel or hollow fiber membrane length (mm)	60	30–90 (±50%)	60	30–90 (±50%)

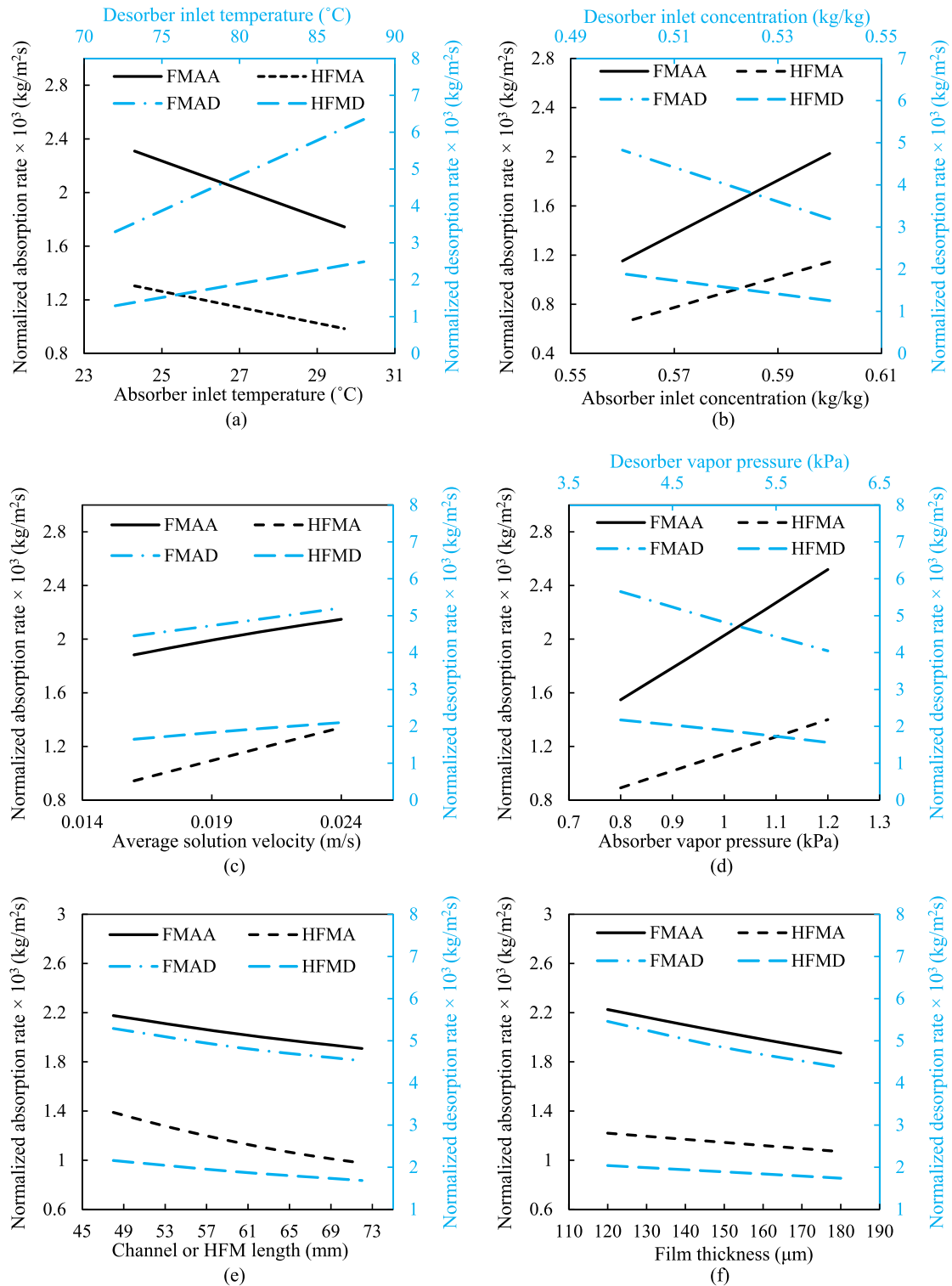


Fig. 3. Absorption and desorption rates versus: (a) solution inlet temperature; (b) solutions inlet concentration; (c) wall temperature; (d) average velocity; (e) vapor pressure; and (f) film thickness. **HFMA:** Hollow Fiber Membrane-based Absorber; **HFMD:** Hollow Fiber Membrane-based Desorber; **FMAA:** Flat Membrane-based Adiabatic Absorber; and **FMAD:** Flat Membrane-based Adiabatic Desorber.

rates are studied. Baseline operating conditions and the physical properties of membrane were arbitrarily selected based on the operating conditions used in the studies available in the literature [27–29,34] – and are listed in Table 6. The selected ranges for this parametric study are selected based on two criteria: i) practicality; and ii) prevention of crystallization. The solution properties mentioned in Table 4 are used for this parametric study. It should be noted that the cross-section area for both flat and hollow fiber membrane-based sorber beds are considered the same in order to have an identical mass flow rate in both systems.

Fig. 3 shows the impact of the solution inlet temperature and concentration, solution mean velocity, water vapor pressure, channel (or hollow fiber membrane) length, and film thickness (or hollow fiber membrane radius) on the absorption rate. The following can be observed:

- i) The desorption rate is higher than the absorption rate since the driving force for mass transfer is higher in the desorption process. The driving force is the difference between the water vapor and water vapor partial pressure at the solution-membrane interface ($|p_v - p_{inf}|$).
- ii) During the absorption process, decreasing the solution inlet temperature, film thickness (or hollow fiber membrane radius) and channel (or hollow fiber membrane) length results in higher absorption rates, while increasing the solution inlet concentration, water vapor pressure and average velocity enhances the absorption rate.
- iii) During the desorption process, increasing the solution inlet temperature, and average velocity leads to higher desorption rates, while decreasing the solution inlet concentration, water vapor pressure, film thickness (or hollow fiber membrane radius), and channel (or hollow fiber membrane) length enhances the desorption rate.
- iv) The solution inlet concentration has the most significant effect on the absorption rate since the variation in the solution concentration significantly changes the water vapor partial pressure at the solution-membrane interface.
- v) The solution velocity has the least effect on the absorption rate since rate since mass diffusion controls the process and the Reynolds number is fairly small ($Re \approx 1$).
- vi) Under identical conditions, the absorption rate of a flat membrane-based sorber bed is higher than that of the hollow fiber membrane-based sorber bed.

Fig. 4 shows the effect of membrane porosity, mean pore diameter, and thickness on absorption rate. The following can be observed:

- i) As expected, increasing the membrane porosity leads to higher absorption rates.
- ii) Decreasing the membrane thickness results in higher absorption rates.
- iii) Increasing the mean pore diameter leads to higher absorption rates.
- iv) Membrane porosity has the most significant influence on the absorption rate.

Table 7 lists the normalized absorption rate for both the absorption and desorption processes. The solution concentration has the greatest effect on the absorption rate.

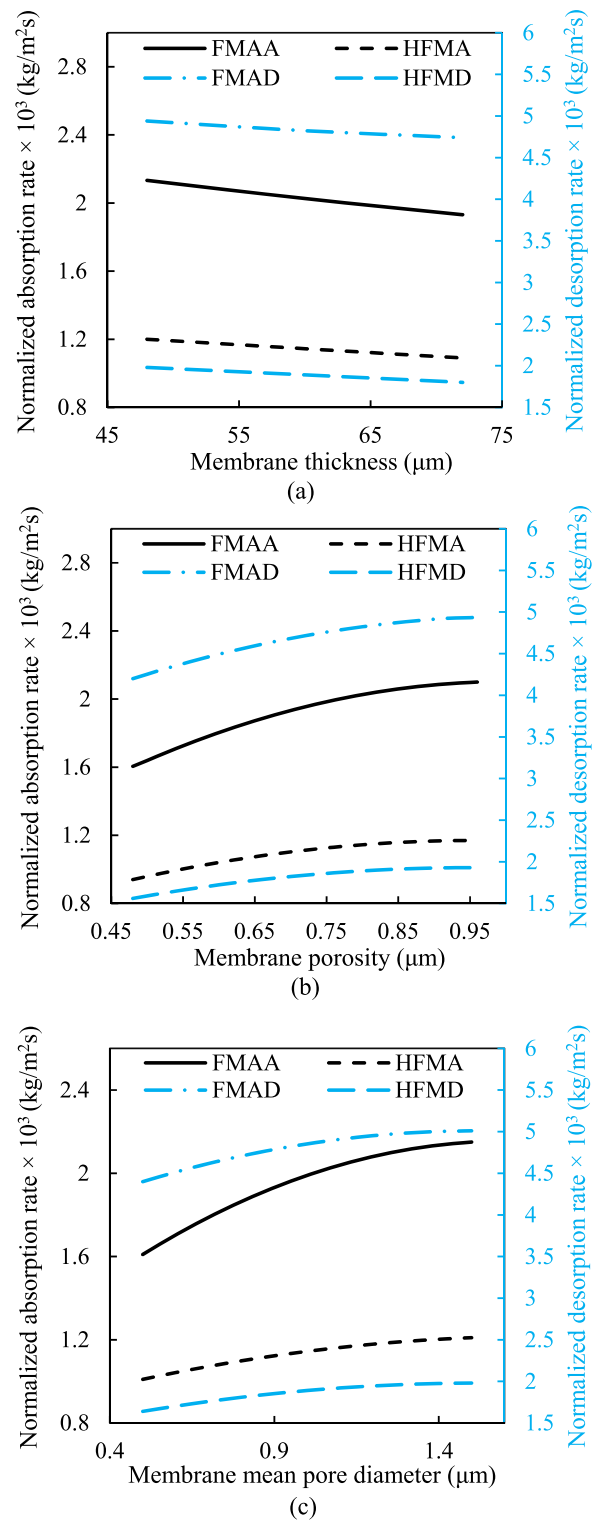


Fig. 4. Absorption rate versus: (a) membrane thickness; (b) membrane porosity; and (c) membrane mean pore diameter. **HFMA**: Hollow Fiber Membrane-based Absorber; **HFMD**: Hollow Fiber Membrane-based Desorber; **FMAA**: Flat Membrane-based Adiabatic Absorber; and **FMAD**: Flat Membrane-based Adiabatic Desorber.

Table 7
Normalized absorption and desorption rates variation for different parameters.

Parameter	Parameter variation (%)	Normalized absorption rate variation (%)		Normalized desorption rate variation (%)	
		Flat membrane	Hollow fiber membrane	Flat membrane	Hollow fiber membrane
Inlet temperature	20	27.8	27.4	63.1	63.4
Inlet concentration	10	108.6	106.7	82.4	80.1
Average velocity	40	6.4	17.3	7.6	11.8
Vapor pressure	40	24	22.3	16.5	15.1
Channel or hollow fiber membrane length	40	6.5	17.6	7.7	12.6
Film thickness	40	8.6	7.4	11.6	7.8
Membrane thickness	100	2.3	2.1	1.2	2
Membrane porosity	60	11.2	8.3	6.6	7.8
Membrane mean pore diameter	100	5.2	3.2	2.4	3.3

5. Conclusion

In this study, two novel analytical solutions were developed for heat and mass transfer in the flat and hollow fiber membrane-based adiabatic sorber beds used in absorption chillers and heat pumps. The present models were validated with the available numerical studies and experimental data. In addition, a parametric study was carried out to investigate the impact of the operating conditions and physical properties of membrane on the absorption rate. The main findings of this study could be summarized as follows:

- The solution inlet concentration is the most effective parameter for increasing the absorption rate while the solution velocity is the least effective parameter.
- Porosity is the most important membrane property for increasing the absorption rate while the membrane thickness has the least effect.
- The desorption rate is higher than the absorption rate due to the higher mass transfer driving force during desorption ($|p_v - p_{inf}|$).
- The absorption rate of a flat membrane-based sorber bed is up to two times higher than that of a hollow fiber membrane-based sorber bed under the same operating conditions

Author statement

Mahyar Ashouri: Conceptualization, Analytical solution, Investigation, Software, Writing - original draft.
Majid Bahrami: Conceptualization, Writing - review & editing, Supervision, Project administration, Funding acquisition.

Declaration of Competing Interest

The authors declare that they have no known competing financial interests or personal relationships that could have appeared to influence the work reported in this paper.

Data Availability

No data was used for the research described in the article.

Acknowledgements

This research is supported by funding from the Pacific Institute for Climate Solutions (PICS) Opportunity Grant (No. 36170–50280) and the Natural Sciences and Engineering Research Council of Canada (NSERC) Advancing Climate Change Science in Canada Grant (No. 536076–18). We acknowledge the support of the Natural Sciences and Engineering Research Council of Canada (NSERC) Collaborative Research and Training Experience program, CREATE (No. 554770–2021). This work made use of the 4D LABS shared facilities supported by the Canada Foundation for Innovation (CFI),

British Columbia Knowledge Development Fund (BCKDF), Western Economic Diversification Canada (WD) and Simon Fraser University (SFU).

Appendix. A. LiBr-water equilibrium state equation constants

The following parameters are used to calculate the water vapor partial pressure of aqueous LiBr (see Eq. (17)), and their corresponding constants are presented in Table A.1.

$$A = a_1 + a_2c_{inf} + a_3c_{inf}^2 \tag{A.1a}$$

$$B = a_4 + a_5c_{inf} + a_6c_{inf}^2 \tag{A.1b}$$

$$C = a_7 + a_8c_{inf} + a_9c_{inf}^2 \tag{A.1c}$$

Appendix. B. The similarity solution for flat membrane-based adiabatic sorber beds

The similarity solution is used to develop an analytical model for heat and mass transfer in a flat membrane-based adiabatic sorber bed. Analogous to the procedure mentioned in Ref. [45], the mean temperature and concentration at the solution-membrane interface are defined as follows [45]:

$$\bar{\theta}_{inf} = \frac{1}{\bar{\xi}} \int_0^{\bar{\xi}} \theta_{inf} d\bar{\xi} \tag{B.1}$$

$$\bar{\gamma}_{inf} = \frac{1}{\bar{\xi}} \int_0^{\bar{\xi}} \gamma_{inf} d\bar{\xi} \tag{B.2}$$

Instead of Eqs. (15) and (19), Eqs. (B.1) and (B.2) are applied to the boundary conditions at the solution-membrane interface. The temperature and concentration partial differential equations (Eqs. (6) and (7)) are converted to ordinary differential equations (Eqs. (B.3) and (B.4)) using the self-similar variable mentioned in Eq. (B.5) [47]:

$$\frac{d^2\theta}{d\zeta^2} + \zeta \frac{d\theta}{d\zeta} = 0 \tag{B.3}$$

$$\frac{d^2\gamma}{d\zeta^2} + Le\zeta \frac{d\gamma}{d\zeta} = 0 \tag{B.4}$$

Table A.1
Constants of Eq. (17) for water vapor partial pressure of aqueous LiBr [44].

Constant	Value	Constant	Value
a_1	0.8941	a_6	-1307.8
a_2	17.742	a_7	-238.710
a_3	-12.236	a_8	-42.641
a_4	339.1	a_9	234,240
a_5	-2193.8		

$$\zeta = \frac{\eta}{\sqrt{2\xi}} \tag{B.5}$$

By applying the boundary conditions (Eqs. (B.1) and (B.2)), the analytical solutions to Eqs. (B.3) and (B.4) are as follows [47]:

$$\theta(\xi, \eta) = \bar{\theta}_{inf} \left[1 - \operatorname{erf} \left(\frac{\eta}{2\sqrt{\xi}} \right) \right] \tag{B.6}$$

$$\gamma(\xi, \eta) = \bar{\gamma}_{inf} \left[1 - \operatorname{erf} \left(\frac{\sqrt{Le}}{2} \frac{\eta}{\sqrt{\xi}} \right) \right] \tag{B.7}$$

To obtain the mean temperature and concentration values, Eqs. (B.6) and (B.7) are coupled at the solution-membrane interface using Eqs. (15) and (19). By averaging the boundary conditions at the solution-membrane interface (Eqs. (15) and (19)) with respect to variable "z" and given the definition of the mean temperature and concentration (Eqs. (B.1) and (B.2)), the following equations are found:

$$\frac{b_3}{\xi} \int_0^\xi \frac{\partial \gamma}{\partial \eta} |_{inf} d\tilde{\xi} = k_m(p_v - b_4\bar{\theta}_{inf} - b_5\bar{\gamma}_{inf} - p_o) \tag{B.8}$$

$$\frac{1}{\xi} \int_0^\xi \frac{\partial \theta}{\partial \eta} |_{inf} d\tilde{\xi} = \frac{\Lambda}{Le} \frac{1}{\xi} \int_0^\xi \frac{\partial \gamma}{\partial \eta} |_{inf} d\tilde{\xi} \tag{B.9}$$

By substituting Eqs. (B.6) and (B.7) in Eqs. (B.8) and (B.9), the following equations can be obtained:

$$-\bar{\gamma}_{inf} \sqrt{\frac{Le}{\pi}} \frac{b_3}{\xi} \int_0^\xi \frac{1}{\sqrt{\xi}} d\tilde{\xi} = k_m(p_v - b_4\bar{\theta}_{inf} - b_5\bar{\gamma}_{inf} - p_o) \tag{B.10}$$

$$\bar{\theta}_{inf} \int_0^\xi \frac{1}{\sqrt{\xi}} d\tilde{\xi} = \frac{\Lambda}{Le} \bar{\gamma}_{inf} \int_0^\xi \frac{1}{\sqrt{\xi}} d\tilde{\xi} \tag{B.11}$$

By solving the systems of Eqs. (B.10) and (B.11), the mean temperature and concentration at the solution-membrane interface are obtained:

$$\bar{\theta}_{inf} = \frac{\Lambda}{\sqrt{Le}} \left[\frac{k_m(p_v - p_o)}{k_m b_5 + 2 \frac{b_3 \sqrt{Le}}{\sqrt{\pi \xi}} + \frac{k_m b_4 \Lambda}{\sqrt{Le}}} \right] \tag{B.12}$$

$$\bar{\gamma}_{inf} = \frac{k_m(p_v - p_o)}{k_m b_5 + 2 \frac{b_3 \sqrt{Le}}{\sqrt{\pi \xi}} + \frac{k_m b_4 \Lambda}{\sqrt{Le}}} \tag{B.13}$$

The temperature and concentration profiles are as follows:

$$\theta(\xi, \eta) = \frac{\Lambda}{\sqrt{Le}} \left[\frac{k_m(p_v - p_o)}{k_m b_5 + 2 \frac{b_3 \sqrt{Le}}{\sqrt{\pi \xi}} + \frac{k_m b_4 \Lambda}{\sqrt{Le}}} \right] \left[1 - \operatorname{erf} \left(\frac{\eta}{2\sqrt{\xi}} \right) \right] \tag{B.14}$$

$$\gamma(\xi, \eta) = \left[\frac{k_m(p_v - p_o)}{k_m b_5 + 2 \frac{b_3 \sqrt{Le}}{\sqrt{\pi \xi}} + \frac{k_m b_4 \Lambda}{\sqrt{Le}}} \right] \left[1 - \operatorname{erf} \left(\frac{\sqrt{Le}}{2} \frac{\eta}{\sqrt{\xi}} \right) \right] \tag{B.15}$$

Appendix C. The Laplace transform method for hollow fiber membrane-based sorber beds

The Laplace transform method is used to develop an analytical model for heat and mass transfer in hollow fiber membrane-based adiabatic sorber bed. By taking the Laplace transform with respect

to "z", the initial and boundary conditions (Eqs. (12) to (15)) are transformed to:

$$\frac{\partial \Theta(s, \eta = 0)}{\partial \eta} = 0 \tag{C.1}$$

$$\frac{\partial Y(s, \eta = 0)}{\partial \eta} = 0 \tag{C.2}$$

$$b_3 \frac{\partial Y(s, \eta = 1)}{\partial \eta} |_{inf} = k_m((p_v - p_o)/s - b_4\Theta(s, \eta = 1) - b_5Y(s, \eta = 1)) \tag{C.3}$$

$$\frac{\partial \Theta(s, \eta = 1)}{\partial \eta} |_{inf} = \frac{\Lambda}{Le} \frac{\partial Y(s, \eta = 1)}{\partial \eta} |_{inf} \tag{C.4}$$

Similarly, by taking the Laplace transform of Eqs. (6) and (7):

$$s \cdot \Theta = \frac{d^2 \Theta}{d\eta^2} + \frac{1}{\eta} \frac{d\Theta}{d\eta} \tag{C.5}$$

$$s \cdot Le \cdot Y = \frac{d^2 Y}{d\eta^2} + \frac{1}{\eta} \frac{dY}{d\eta} \tag{C.6}$$

The solutions to Eqs. (C.5) and (C.6) can be found based on the first and second kind of the modified Bessel function:

$$\Theta(s, \eta) = c_1 I_0(\sqrt{s}\eta) + c_2 K_0(\sqrt{s}\eta) \tag{C.7}$$

$$Y(s, \eta) = c_3 I_0(\sqrt{Le \cdot s}\eta) + c_4 K_0(\sqrt{Le \cdot s}\eta) \tag{C.8}$$

c₂ and c₄ should be zero to prevent a singularity at η = 0. By substituting Eqs. (C.7) and (C.8) in Eqs. (C.3) and (C.4), the following equations can be obtained:

$$b_3 c_3 \sqrt{Le \cdot s} I_1(\sqrt{Le \cdot s}) = k_m((p_v - p_o)/s - b_4 c_1 I_0(\sqrt{s}) - b_5 c_3 I_0(\sqrt{Le \cdot s})) \tag{C.9}$$

$$c_1 \sqrt{s} I_1(\sqrt{s}) = \frac{\Lambda}{Le} c_3 \sqrt{Le \cdot s} I_1(\sqrt{Le \cdot s}) \tag{C.10}$$

Thus, c₁ and c₃ are obtained as follows:

$$c_1 = \frac{\Lambda}{\sqrt{Le}} \frac{I_1(\sqrt{Le \cdot s})}{I_1(\sqrt{s})} c_3 \tag{C.11}$$

$$c_3 = \frac{k_m(p_v - p_o)/s}{b_3 \sqrt{Le \cdot s} I_1(\sqrt{Le \cdot s}) + k_m b_4 \frac{\Lambda}{\sqrt{Le}} \frac{I_1(\sqrt{Le \cdot s})}{I_1(\sqrt{s})} I_0(\sqrt{s}) + k_m b_5 I_0(\sqrt{Le \cdot s})} \tag{C.12}$$

The temperature and concentration in the Laplace space are expressed as follows:

$$\Theta(s, \eta) = \left[\frac{\Lambda}{\sqrt{Le}} \frac{I_1(\sqrt{Le \cdot s})}{I_1(\sqrt{s})} \right] \times \left[\frac{k_m(p_v - p_o)}{b_3 \sqrt{Le \cdot s} I_1(\sqrt{Le \cdot s}) + k_m b_4 \frac{\Lambda}{\sqrt{Le}} \frac{I_1(\sqrt{Le \cdot s})}{I_1(\sqrt{s})} I_0(\sqrt{s}) + k_m b_5 I_0(\sqrt{Le \cdot s})} \right] I_0(\sqrt{s}\eta) \tag{C.13}$$

$$Y(s, \eta) = \left[\frac{k_m(p_v - p_o)}{b_3 \sqrt{Le \cdot s} I_1(\sqrt{Le \cdot s}) + k_m b_4 \frac{\Lambda}{\sqrt{Le}} \frac{I_1(\sqrt{Le \cdot s})}{I_1(\sqrt{s})} I_0(\sqrt{s}) + k_m b_5 I_0(\sqrt{Le \cdot s})} \right] I_0(\sqrt{Le \cdot s}\eta) \tag{C.14}$$

Finally, by taking the inverse Laplace transform from Eqs. (C.11) and (C.12) using the Stehfest method [43], the temperature and concentration profiles are found [48]:

$$\theta(\xi, \eta) = \frac{\ln 2}{\xi} \sum_{i=1}^N V_i \Theta\left(\frac{\ln 2}{\xi} i, \eta\right) \quad (\text{C.15})$$

$$\gamma(\xi, \eta) = \frac{\ln 2}{\xi} \sum_{i=1}^N V_i Y\left(\frac{\ln 2}{\xi} i, \eta\right) \quad (\text{C.16})$$

where, V_i is defined as follows:

$$V_i = (-1)^{\frac{N}{2}+j} \frac{\sum_{k=\lfloor \frac{i-1}{2} \rfloor}^{\min(j, \frac{N}{2})} k^{\frac{N}{2}} (2k)!}{\left(\frac{N}{2} - k\right)! k! (k-1)! (j-k)! (2k-j)!} \quad (\text{C.17})$$

To calculate the above-mentioned series, "N" equal to 100 is enough.

References

- [1] D. Ürge-Vorsatz, L.F. Cabeza, S. Serrano, C. Barreneche, K. Petrichenko, Heating and cooling energy trends and drivers in buildings, *Renew. Sustain. Energy Rev.* 41 (2015) 85–98.
- [2] A. Salari, M. Ashouri, A. Hakkaki-Fard, On the performance of inclined rooftop solar chimney integrated with photovoltaic module and phase change material: a numerical study, *Sol. Energy*. 211 (2020) 1159–1169.
- [3] M. Ashouri, A. Hakkaki-Fard, Improving the performance of the finned absorber inclined rooftop solar chimney combined with composite PCM and PV module, *Sol. Energy*. 228 (2021) 562–574, doi:10.1016/J.SOLENER.2021.09.088.
- [4] F. Pardo, G. Zarca, A. Urriaga, Effect of feed pressure and long-term separation performance of Pebax-ionic liquid membranes for the recovery of difluoromethane (R32) from refrigerant mixture R410A, *J. Memb. Sci.* 618 (2021) 118744, doi:10.1016/J.MEMSCI.2020.118744.
- [5] J.A. Bush, J. Vanneste, D. Leavitt, J. Bergida, M. Krzmarzick, S.-J. Kim, C. Ny, T.Y. Cath, Membrane distillation crystallization of ammonium nitrate solutions to enable sustainable cold storage: electrical conductivity as an in-situ saturation indicator, *J. Memb. Sci.* 631 (2021) 119321.
- [6] C. Forman, I.K. Muritala, R. Pardemann, B. Meyer, Estimating the global waste heat potential, *Renew. Sustain. Energy Rev.* 57 (2016) 1568–1579.
- [7] M. Rouhani, M. Bahrami, Effective thermal conductivity of packed bed adsorbers: part 2- Theoretical model, *Int. J. Heat Mass Transf.* 123 (2018) 1212–1220.
- [8] A.H.H. Ali, P. Schwerdt, Characteristics of the membrane utilized in a compact absorber for lithium bromide–water absorption chillers, *Int. J. Refrig.* 32 (2009) 1886–1896.
- [9] J. Woods, J. Pellegrino, E. Kozubal, S. Slayzak, J. Burch, Modeling of a membrane-based absorption heat pump, *J. Memb. Sci.* 337 (2009) 113–124.
- [10] J. Ibarra-Bahena, S. Raman, Y.R. Galindo-Luna, A. Rodríguez-Martínez, W. Rivera, Role of membrane technology in absorption heat pumps: a comprehensive review, *Membranes* 10 (2020) 216.
- [11] S.-M. Huang, Heat and mass transfer in a quasi-counter flow parallel-plate membrane-based absorption heat pump (QPMAHP), *J. Memb. Sci.* 496 (2015) 39–47.
- [12] S.-M. Huang, M. Yang, W.-H. Huang, S. Tao, B. Hu, F.G.F. Qin, An analytical solution of heat and mass transfer in a counter/parallel flow plate membrane module used in an absorption heat pump, *Int. J. Therm. Sci.* 124 (2018) 110–121.
- [13] Q. Shen, D. Sun, Y. Xu, T. Jin, X. Zhao, N. Zhang, K. Wu, Z. Huang, Natural convection heat transfer along vertical cylinder heat sinks with longitudinal fins, *Int. J. Therm. Sci.* 100 (2016) 457–464.
- [14] R.N. Isfahani, S. Moghaddam, Absorption characteristics of lithium bromide (LiBr) solution constrained by superhydrophobic nanofibrous structures, *Int. J. Heat Mass Transf.* 63 (2013) 82–90.
- [15] S. Bigham, D. Yu, D. Chugh, S. Moghaddam, Moving beyond the limits of mass transport in liquid adsorbent microfilms through the implementation of surface-induced vortices, *Energy*. 65 (2014) 621–630. 10.1016/J.ENERGY.2013.11.068.
- [16] M. De Vega, N. García-Hernando, M. Venegas, Experimental performance of membrane water absorption in LiBr solution with and without cooling, *Appl. Therm. Eng.* 180 (2020) 115786.
- [17] D. Yu, J. Chung, S. Moghaddam, Parametric study of water vapor absorption into a constrained thin film of lithium bromide solution, *Int. J. Heat Mass Transf.* 55 (2012) 5687–5695, doi:10.1016/J.IJHEATMASSTRANSFER.2012.05.064.
- [18] F. Asfand, Y. Stiriba, M. Bourouis, CFD simulation to investigate heat and mass transfer processes in a membrane-based absorber for water-LiBr absorption cooling systems, *Energy* 91 (2015) 517–530, doi:10.1016/J.ENERGY.2015.08.018.
- [19] J. Woods, J. Pellegrino, E. Kozubal, J. Burch, Design and experimental characterization of a membrane-based absorption heat pump, *J. Memb. Sci.* 378 (2011) 85–94.
- [20] F. Abdollahi, S.A. Hashemifard, A. Khosravi, T. Matsuura, Heat and mass transfer modeling of an energy efficient hybrid membrane-based air conditioning system for humid climates, *J. Memb. Sci.* 625 (2021) 119179.
- [21] Z. Sui, C. Zhai, W. Wu, Swirling flow for performance improvement of a microchannel membrane-based absorber with discrete inclined grooves, *Int. J. Refrig.* (2021).
- [22] C. Zhai, W. Wu, Energetic, exergetic, economic, and environmental analysis of microchannel membrane-based absorption refrigeration system driven by various energy sources, *Energy* 239 (2022) 122193.
- [23] C. Zhai, W. Wu, Experimental evaluation on heat/mass transfer and pressure drop of a microchannel membrane-based desorber for compact and efficient H₂O/LiBr absorption refrigeration, *Int. J. Heat Mass Transf.* 195 (2022) 123198.
- [24] Z. Sui, C. Zhai, W. Wu, Parametric and comparative study on enhanced microchannel membrane-based absorber structures for compact absorption refrigeration, *Renew. Energy* 187 (2022) 109–122.
- [25] C. Zhai, Y. Sui, Z. Sui, W. Wu, Ionic liquids for microchannel membrane-based absorption heat pumps: performance comparison and geometry optimization, *Energy Convers. Manag.* 239 (2021) 114213.
- [26] C. Zhai, W. Wu, A. Coronas, Membrane-based absorption cooling and heating: development and perspectives, *Renew. Energy* 177 (2021) 663–688.
- [27] M. Venegas, M. de Vega, N. García-Hernando, U. Ruiz-Rivas, Adiabatic vs non-adiabatic membrane-based rectangular micro-absorbers for H₂O-LiBr absorption chillers, *Energy*. 134 (2017) 757–766. 10.1016/J.ENERGY.2017.06.068.
- [28] N. García-Hernando, M. Venegas, M. De Vega, Experimental performance comparison of three flat sheet membranes operating in an adiabatic microchannel absorber, *Appl. Therm. Eng.* 152 (2019) 835–843.
- [29] N. García-Hernando, M. De Vega, M. Venegas, Experimental characterisation of a novel adiabatic membrane-based micro-absorber using H₂O-LiBr, *Int. J. Heat Mass Transf.* 129 (2019) 1136–1143.
- [30] J.M. Vadillo, D. Hospital-Benito, C. Moya, L. Gomez-Coma, J. Palomar, A. Garea, A. Ibarren, Modelling and simulation of hollow fiber membrane vacuum regeneration for CO₂ desorption processes using ionic liquids, *Sep. Purif. Technol.* 277 (2021) 119465.
- [31] J. Chen, H. Chang, S.-R. Chen, Simulation study of a hybrid absorber–heat exchanger using hollow fiber membrane module for the ammonia–water absorption cycle, *Int. J. Refrig.* 29 (2006) 1043–1052.
- [32] M. Berdasco, A. Coronas, M. Vallès, Study of the adiabatic absorption process in polymeric hollow fiber membranes for ammonia/water absorption refrigeration systems, *Appl. Therm. Eng.* 137 (2018) 594–607.
- [33] S.J. Hong, E. Hihara, C. Dang, Mass recovery characteristics of hydrophobic hollow fiber membrane-based refrigerant mass exchangers in vapor absorption refrigeration systems, *J. Memb. Sci.* 580 (2019) 177–189.
- [34] S.J. Hong, E. Hihara, C. Dang, Analysis of adiabatic heat and mass transfer of microporous hydrophobic hollow fiber membrane-based generator in vapor absorption refrigeration system, *J. Memb. Sci.* 564 (2018) 415–427.
- [35] Z. Wang, Z. Gu, S. Feng, Y. Li, Application of vacuum membrane distillation to lithium bromide absorption refrigeration system, *Int. J. Refrig.* 32 (2009) 1587–1596.
- [36] A.M. Elsaifi, M. Ashouri, M. Bahrami, A similarity solution for laminar forced convection heat transfer from solid spheres, *Int. J. Heat Mass Transf.* 196 (2022) 123310.
- [37] L.-Z. Zhang, An analytical solution to heat and mass transfer in hollow fiber membrane contactors for liquid desiccant air dehumidification, *J. Heat Transfer*. 133 (2011).
- [38] R. Wang, D.F. Li, D.T. Liang, Modeling of CO₂ capture by three typical amine solutions in hollow fiber membrane contactors, *Chem. Eng. Process. Process Intensif.* 43 (2004) 849–856.
- [39] S. Zha, J. Yu, G. Zhang, N. Liu, R. Lee, Polyethersulfone (PES)/cellulose acetate butyrate (CAB) composite hollow fiber membranes for BTEX separation from produced water, *RSC Adv* 5 (2015) 105692–105698.
- [40] M. Ashouri, M. Bahrami, Analytical solution for coupled heat and mass transfer in membrane-based absorbers, *Int. J. Heat Mass Transf.* 192 (2022) 122892.
- [41] T.L. Bergman, F.P. Incropera, D.P. DeWitt, A.S. Lavine, *Fundamentals of Heat and Mass Transfer*, John Wiley & Sons, 2011.
- [42] E.A. Mason, M. EA, M. AP, Gas transport in porous media: the dusty-gas model, (1983).
- [43] Y. Wu, Simultaneous heat and mass transfer in laminar falling film on the outside of a circular tube, *Int. J. Heat Mass Transf.* 93 (2016) 1089–1099.
- [44] A. Matsuda, T. Munakata, T. Yoshimaru, T. Kubara, H. Fuchi, Measurement of vapor-pressures of lithium bromide water solutions, *Kagaku Kogaku Ronbunshu* 6 (1980) 119–122.
- [45] T. Meyer, F. Ziegler, Analytical solution for combined heat and mass transfer in laminar falling film absorption using first type boundary conditions at the interface, *Int. J. Heat Mass Transf.* 73 (2014) 141–151.
- [46] N. Giannetti, S. Yamaguchi, K. Saito, Simplified expressions of the transfer coefficients on a partially wet absorber tube, *Int. J. Refrig.* 105 (2019) 135–147, doi:10.1016/j.ijrefrig.2018.07.007.
- [47] V.E. Nakoryakov, N.I. Grigoreva, Heat and mass transfer in film absorption with varying liquid-phase volume, *Theor. Found. Chem. Eng.* 29 (1995).
- [48] M. Ashouri, M. Bahrami, Heat and mass transfer in laminar falling film absorption: a compact analytical model, *Int. J. Heat Mass Transf.* 188 (2022) 122598.